processing of the antenna arrays. The authors also extend many thanks to P. Delmotte, ESAT, Leuven, Belgium, for his assistance during the far-field measurements.

REFERENCES

[1] H. Legay and L. Shafai, "A self-matching wide-band feed network for microstrip arrays," *IEEE Trans. Antennas Propagat.*, vol. 45, pp. 715–722, Apr. 1997.

[2] P. S. Hall and C. M. Hall, "Coplanar corporate feed effects in microstrip patch array design," *Proc. Inst. Elect. Eng.*, pt. H, vol. 135, pp. 180–186, June 1988.

[3] E. A. Soliman, S. Brebels, G. A. E. Vandenbosch, and E. Beyne, "X-band brick wall antenna fed by CPW," *Electron. Lett.*, vol. 34, pp. 836–838, Apr. 1998.

[4] H.-C. Liu, T.-S. Horng, and N. G. Alexopoulos, "Radiation of printed antennas with a coplanar waveguide feed," *IEEE Trans. Antennas Propagat.*, vol. 43, pp. 1143–1148, Oct. 1995.

[5] E. A. Soliman, P. Pieters, E. Beyne, and G. A. E. Vandenbosch, "Suppression of the parasitic modes in CPW discontinuities using MCM-D technology-application to a novel 3-dB power splitter," *IEEE Trans. Microwave Theory Tech.*, vol. 46, pp. 2426–2430, Dec. 1998.

[6] G. A. E. Vandenbosch and A. R. Van de Capelle, "Use of subsectional edge expansion functions (SEEF's) to analyze rectangular microstrip antennas with the method of moments," *Proc. Inst. Elect. Eng.*, pt. H, vol. 139, pp. 159–164, Apr. 1992.

[7] E. Levine, "Special measurement techniques for printed antennas," in *Handbook of Microstrip Antennas*, J. R. James and P. S. Hall, Eds. Stevenage, U.K.: Peregrinus, 1989, ch. 16, p. 991.

On the Significance of Envelope Peak-to-Average Ratio for Estimating the Spectral Regrowth of an RF/Microwave Power Amplifier

John F. Sevic and Michael B. Steer

Abstract—The peak-to-average ratio (PAR) of a signal is commonly used for estimating the backoff required for an radio-frequency/microwave power amplifier to exhibit acceptable intermodulation distortion. In this paper, it is shown that the PAR is an inaccurate metric for predicting the backoff and can lead to improper choices for modulation with respect to the linearity–efficiency tradeoff. A specific case is presented, based on the IS-94 code-division multiple-access communication (CDMA) reverse-link and IS-95 CDMA forward-link wireless standards. Using simulation and load–pull measurements, it is illustrated that although quaternary phase-shift keying has a higher PAR than offset QPSK (O-QPSK), it has lower adjacent-channel power, for constant average power. This observation, contrary to what is expected, is explained by introducing the envelope distribution function, which characterizes the saturation of an amplifier based on the time-domain statistics of the applied signal.

Index Terms—Digital modulation, intermodulation distortion, linearity, microwave power amplifier, peak-to-average ratio, RF power amplifier, signal statistics, spectral regrowth.

I. Introduction

Design of digital communication systems often uses the peak-to-average ratio (PAR) of the modulated signal as a qualitative estimate of the tradeoff between the linearity and efficiency of the transmitter stage. At the circuit level, the design of RF/microwave power amplifiers uses the PAR to estimate the load impedance and gatewidth for acceptable intermodulation (IM) distortion and required average output power. For a given average power, the PAR indicates the maximum instantaneous state of saturation of the power amplifier and is, thus, directly related to the IM distortion generated, which, for digitally modulated signals, is manifested as spectral regrowth. Analytical derivation of this relationship is difficult, except for simplistic nonlinearities, and most often one finds that the PAR is used to estimate the required output backoff from the 1-dB single-tone saturation point, particularly for system-level design. Since efficiency decreases as average power is reduced from the saturated-power point, customary application of this metric indicates that a signal with a high PAR would result in lower amplifier efficiency than one with a lower PAR. Thus, from an efficiency perspective, a low PAR modulation would appear to be desirable.

If average IM distortion can be considered as a summation of many instantaneous saturation events, it follows that the resultant average IM distortion must depend on the statistical properties of the signal envelope. The more often an envelope induces saturation, independent of the PAR, then the greater the average IM distortion generated. There are two significant consequences of this observation. The first is that the average IM distortion generated by a power amplifier must depend not only on what the peak power is, as specified by the PAR, but also on the variance of the instantaneous power about the mean power. The second consequence is that since the PAR itself does not characterize how often the associated peak power occurs, it is incapable of characterizing the resultant average IM characteristics. Indeed, it is for these reasons why relating adjacent-channel power ratio (ACPR) to two-tone IM correlation is, in general, difficult since the envelope statistics are vastly different [1].

In this paper, the spectral regrowth properties of QPSK and offset QPSK (O-QPSK) modulated signals used in the IS-94 CDMA reverse-link and IS-95 CDMA forward-link standards, respectively, are compared [2], [3]. It is shown that conventional PAR analysis, which was the basis for choosing O-QPSK for IS-94, underestimates the associated relative spectral regrowth. To describe the statistical nature of the modulated signal, the envelope distribution function is introduced. This function describes the probability of a peak-power occurring and, hence, the frequency of instantaneous compression of the power amplifier. The envelope distribution function illustrates why spectral regrowth of QPSK, using IS-95 filtering, has lower spectral regrowth than similarly filtered O-QPSK, contrary to what is expected using the PAR. Spectral regrowth simulations of a submicrometer laterally diffused MOS (LDMOS) transistor, under power loading with strong class-AB bias, are used to confirm the predictions of the envelope distribution function. In addition, load–pull measurements of a similar LDMOS transistor, under linearity–efficiency loading and weak class-AB bias, are given, verifying the simulated results under different operating conditions.

II. Generation of Digitally Modulated Signals and the Envelope Distribution Function

Simulation of spectral regrowth is now commonplace; the two most common methods being harmonic-balance envelope-related methods
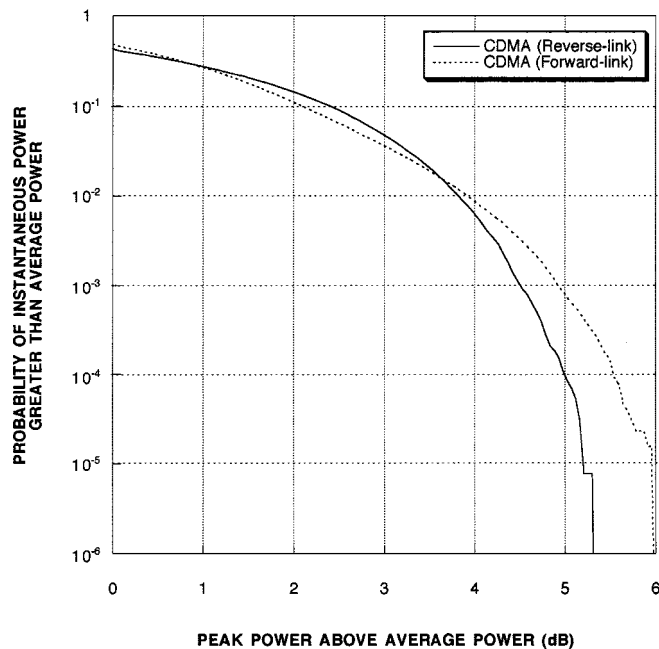
Fig. 1. Envelope distribution functions for IS-95 QPSK and IS-94 O-QPSK modulation.

Fig. 2. Simulated lower ACPR for IS-95 QPSK and IS-94 O-QPSK modulation (computed at an offset of 885 kHz normalized to the total channel power).

Fig. 3. Simulated upper ACPR for IS-95 QPSK and IS-94 O-QPSK modulation (computed at an offset of 885 kHz normalized to the total channel power).

and behavioral-model-related methods[1] [4]–[6]. Since data sequence correlation and filtering each impact the envelope statistics, it is necessary that the signal used in the simulation be identical to that used in the load–pull characterization [7]. The digitally modulated signals used for the present experiment were generated using a proprietary method with the HP Circuit Envelope simulator. The complex envelope from this source was downloaded to an arbitrary waveform generator coupled to a vector signal generator, thus providing the digitally modulated signal for load–pull characterization.

To simplify filtering, the sampling rate of the source was set equal to four times the chip rate specified by the IS-94/IS-95 standards, which is the sampling rate of the associated filter. The length of the pilot-tone spreading sequence was approximated using 2^9 b, with the maximal length sequence (MLS) coefficients and seed values specified by IS-94 [2], [3]. Although this sequence is not as long as the period of the spreading-sequence given in IS-94, it has been found to be statistically identical with respect to stationarity [8].

Representative envelope distribution functions for IS-95 QPSK and IS-94 O-QPSK modulated signals, derived from simulation, are shown in Fig. 1. The envelope distribution function is defined as the probability that the instantaneous power is greater than the average power

$$\Psi(\tilde{p}) = 1 - \int_{E[\tilde{p}]}^{\infty} \varphi(\tilde{p}) \, d\tilde{p} \qquad (1)$$

where $E[\tilde{p}]$ is the average power of the complex envelope $\tilde{p}(t)$ and $\varphi(\tilde{p})$ is the probability density function of $\tilde{p}(t)$. The PAR is defined as the x-axis intercept at a probability of 10^{-6}. Using this definition, the PAR's for IS-95 QPSK and IS-94 O-QPSK are 6.1 and 5.1 dB, respectively, and these are the commonly used values. Since the probability of these peak powers occurring is extremely low, it is obvious that the PAR is not a reliable metric for estimating the efficiency and linearity tradeoff of an RF/microwave power amplifier since the occurrence of an instantaneous saturation event is very unlikely. Instead, Fig. 1 indicates that the IM distortion of a power amplifier under QPSK

[1]Microwave Design System, version b.07.10, Hewlett-Packard Company, Palo Alto, CA 1997.
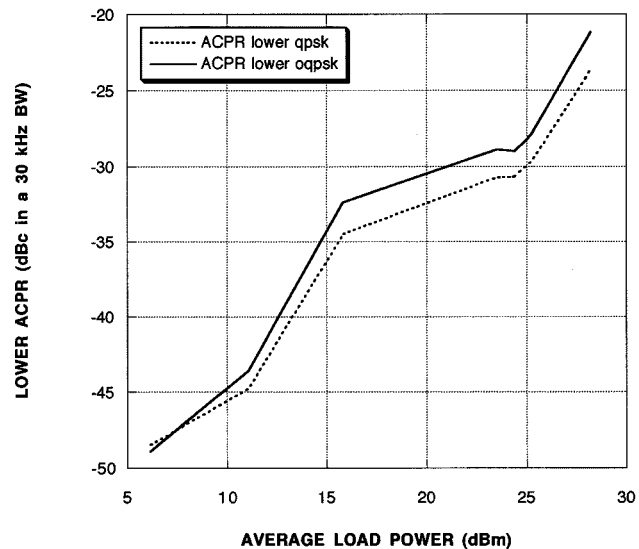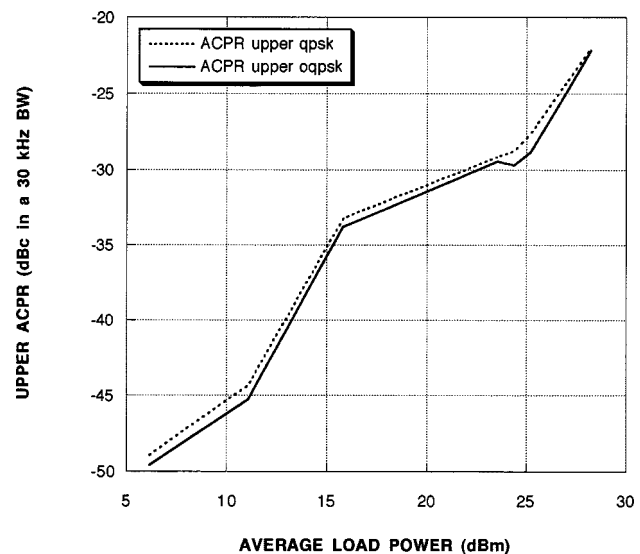
modulation should be better than that with O-QPSK since the envelope distribution function for QPSK rolls off faster in regions of high probability of peak power, i.e., it has a smaller variance in regions of high probability.

III. NONLINEAR SIMULATION AND LOAD–PULL CHARACTERIZATION OF SPECTRAL REGROWTH

A large-signal table-based model was extracted from a unit-cell sub-micrometer LDMOS transistor and was scaled to match the device used in the load–pull characterization. Large-signal verification of the model confirmed acceptable accuracy. The transistor used in the simulation was biased at 4.0 V and 8 mA/mm under maximum power loading, with a carrier frequency of 850 MHz. Figs. 2 and 3 compare simulated lower and upper ACPR's, respectively, for QPSK and O-QPSK excitation. These ACPR's were computed by taking the ratio of the power in a 30-kHz bandwidth, at an offset of 885 kHz, to the total channel power,
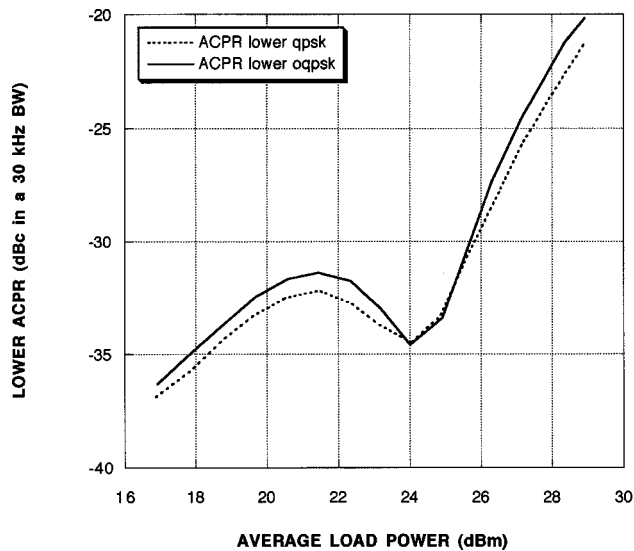
Fig. 4. Measured lower ACPR for IS-95 QPSK and IS-94 O-QPSK modulation (computed at an offset of 885 kHz normalized to the total channel power).
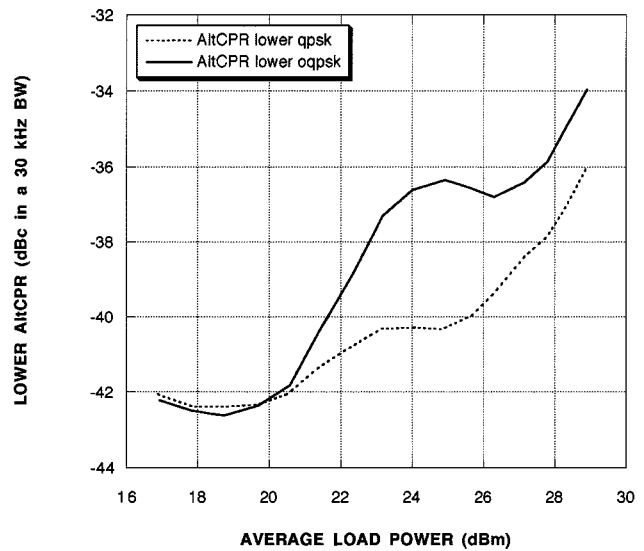
Fig. 6. Measured lower AltCPR for IS-95 QPSK and IS-94 O-QPSK modulation (computed at an offset of 1250 kHz normalized to the total channel power).
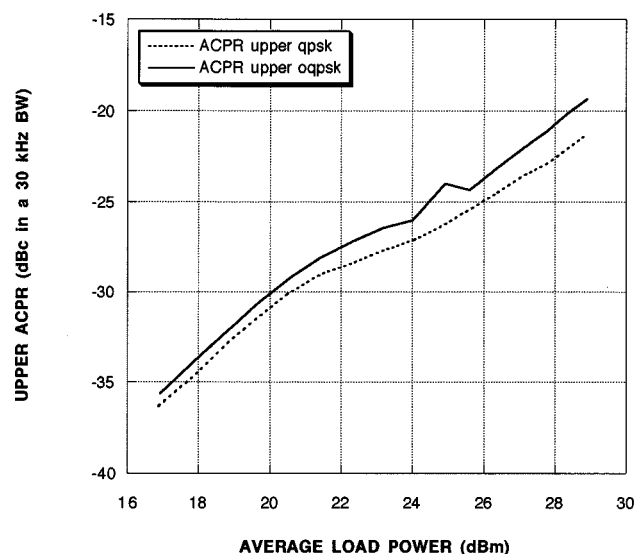
Fig. 5. Measured upper ACPR for IS-95 QPSK and IS-94 O-QPSK modulation (computed at an offset of 885 kHz normalized to the total channel power).
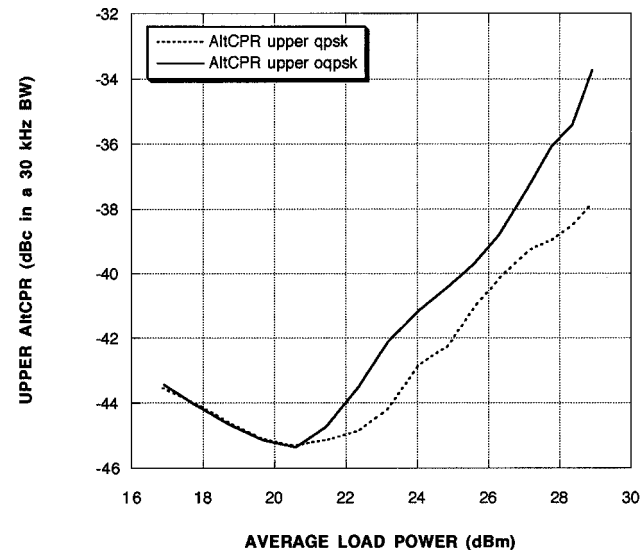
Fig. 7. Measured upper AltCPR for IS-95 QPSK and IS-94 O-QPSK modulation (computed at an offset of 1250 kHz normalized to the total channel power).

using the procedure described in [7]. While the simulated upper QPSK and O-QPSK ACPR's are similar, the lower QPSK ACPR is better than the O-QPSK ACPR by 2 dB from the linear region of the power amplifier well into compression. This behavior is directly attributable to the properties of the envelope distribution function for QPSK, as described in the previous section.

The absence of IM nulling in the simulation is due to inadequate modeling of the envelope termination and the strong class-AB bias of 8 mA/mm [9]. In the simple simulation presented here, the envelope impedance was set to the fundamental frequency impedance. In addition, the quiescent current was chosen higher than what would normally be used to examine the effect of bias current on the linearity relationship between QPSK and O-QPSK. The measured results, presented next, use a more conventional quiescent current of 4 mA/mm.

A transistor identical to the one used in the simulation was evaluated in a Maury load–pull system, with source and load impedances

chosen for optimal linearity–efficiency loading. This was done to further examine the sensitivity of the spectral regrowth relationship between QPSK and O-QPSK under different bias and source/load conditions. The transistor was biased at 4.0 V and 4 mA/mm with a frequency of 850 MHz. An arbitrary waveform generator, using data generated from the simulation, was used to drive a vector signal source, which was directly applied to the load–pull system.

Figs. 4 and 5 compare lower and upper ACPR's, respectively, for QPSK and O-QPSK excitation. Two distinctions can be made between the simulated and measured results. First, unilateral IM nulling is evident in the lower ACPR. Since nulling is not evident in the upper ACPR, the ACPR exhibits asymmetry, which is attributable to the envelope termination effect [9]. The difference in QPSK and O-QPSK ACPR is slightly less than the simulation predicted, although QPSK again exhibits better linearity than O-QPSK.

Figs. 6 and 7 compare lower and upper alternate-channel power ratio (AltCPR), respectively, for QPSK and O-QPSK excitation, measured at

RATIO	QPSK	O-QPSK	IMPROVEMENT
Upper ACPR	-23.0 dB	-21.0 dB	2.0 dB
Lower ACPR	-23.5 dB	-22.6 dB	1.1 dB
Upper AltCPR	-39.1 dB	-36.0 dB	3.1 dB
Lower AltCPR	-37.2 dB	-35.5 dB	2.2 dB

an offset of 1250 kHz [7]. AltCPR also exhibits asymmetry, though the asymmetry is much weaker for QPSK than O-QPSK. QPSK AltCPR is 2–3 dB better than O-QPSK.

Table I summarizes the results for an average load power of 28 dBm. The measured results exhibit an identical trend in spectral regrowth performance to that observed in the simulations. Thus, even under different source/load and bias conditions, QPSK exhibits lower spectral regrowth than O-QPSK. This result is in contradiction to that predicted by PAR's of QPSK and O-QPSK. That is, based on PAR considerations alone, ACPR and AltCPR of QPSK signals would be expected to be much higher than for O-QPSK signals. In fact, just the opposite is observed.

IV. CONCLUSION

A quantitative study of spectral regrowth for QPSK and O-QPSK, representative of the IS-94 and IS-95 CDMA wireless standards, has been presented in this paper. Both nonlinear simulation and measured results indicate that O-QPSK offers no advantage over QPSK in the linearity–efficiency tradeoff of an RF/microwave power amplifier, as would have been predicted using conventional PAR analysis. This perspective, while counter-intuitive in the context of PAR, follows naturally from the envelope distribution function.

The envelope distribution function was introduced as a new figure-of-merit, and clearly illustrates why QPSK, although exhibiting a higher PAR than O-QPSK, exhibits lower spectral regrowth. Although not shown in this paper, simulations using IS-54 $\pi/4\text{-QPSK}$ showed that even with a low PAR of 3.4 dB, the spectral regrowth was larger than similarly filtered QPSK, with a PAR of 4.2 dB. Thus, the conclusions presented are of a general nature, and are not specific to one type of modulation. This new function should find wide application in the design of modulations for optimizing the linearity–efficiency tradeoff of RF/microwave power amplifiers used in digital wireless communication systems.

ACKNOWLEDGMENT

The authors wish to thank the reviewers for their many helpful suggestions.

REFERENCES

[1] J. F. Sevic, M. B. Steer, and A. M. Pavio, "Large-signal automated load–pull of adjacent-channel power for digital wireless communication systems," in *IEEE MTT-S Int. Microwave Symp. Dig.*, June 1996, pp. 763–766.
[2] *Mobile Station-Base Station Compatibility Standard for Dual-Mode Wide-Band Spread Spectrum Cellular System*, EIA/TIA Interim Standard TIA/EIA/IS-94, 1993.
[3] *Mobile Station-Base Station Compatibility Standard for Dual-Mode Wide-Band Spread Spectrum Cellular System*, EIA/TIA Interim Standard TIA/EIA/IS-95, 1993.
[4] J. F. Sevic and J. Staudinger, "Simulation of adjacent-channel power ratio for digital wireless systems," in *IEEE Veh. Technol. Conf. Dig.*, May 1997, pp. 681–685.
[5] K. Gard, H. M. Gutierrez, and M. B. Steer, "Characterization of spectral regrowth in microwave amplifiers based on the nonlinear transformation of complex Gaussian process," *IEEE Trans. Microwave Theory Tech.*, vol. 47, pp. 1059–1069, July 1999.
[6] E. Ngoya and R. Larcheveque, "Envelope transient analysis: A new method for the transient and steady-state analysis of microwave communication circuits and systems," in *IEEE MTT-S Int. Microwave Symp. Dig.*, June 1996, pp. 1365–1368.
[7] J. F. Sevic, M. B. Steer, and A. M. Pavio, "Nonlinear analysis methods for digital wireless communication systems," *Int. J. Microwave Millimeter-Wave Computer-Aided Eng.*, pp. 197–216, May 1996.
[8] J. F. Sevic, "Characterization and simulation of RF/microwave power transistors using digitally modulated signals," in *1998 Fall ARFTG Short-Course Notes*, Dec. 1998.
[9] J. F. Sevic, K. Burger, and M. B. Steer, "A novel load–pull technique for mitigation of envelope-induced ACPR asymmeetry of RF power amplifiers," in *IEEE MTT-S Int. Microwave Symp. Dig.*, June 1998, pp. 601–605.

Three-Dimensional Microwave Tomography: Experimental Imaging of Phantoms and Biological Objects

Serguei Y. Semenov, Alexander E. Bulyshev, Alexandre E. Souvorov, Alexei G. Nazarov, Yuri E. Sizov, Robert H. Svenson, Vitaly G. Posukh, Andrey Pavlovsky, Pavel N. Repin, and George P. Tatsis

Abstract—Microwave tomographic experiments have been performed on a three-dimensional (3-D) phantom and excised canine heart using a 3-D system operating at frequency of 2.4 GHz. A modified gradient reconstruction approach has been employed for the 3-D image reconstruction. To compare two-dimensional (2-D) and 3-D approaches, we also performed 2-D image reconstruction using an approach based on the Newton method. Experimental data acquired on experimental phantoms were analyzed using both 2-D and 3-D reconstruction approaches. High-quality images were reconstructed using the 3-D approach. The reconstruction procedure failed when the 2-D approach was applied to reconstruct images of the 3-D object. An image of the dielectrical properties of the excised canine heart was obtained using a 3-D reconstruction approach. Images successfully revealed a complex internal structure of the heart, including both right-hand side and left-hand side ventricles.

Index Terms—Biophysical experiment, imaging, microwave tomography.